ACS MATERIALS Au
AN OPEN ACCESS JOURNAL OF THE AMERICAN CHEMICAL SOCIETY



pubs.acs.org/materialsau
Article

# Role of Pyridine Nitrogen Position on the Moisture Sensitivity of Organic Emitters

*Published as part of ACS Materials Au special issue "Celebrating the 25th Anniversary of the Chemical Research Society of India".*

Gyana Prakash Nanda, Rajan Suraksha, and Pachaiyappan Rajamalli*

Cite This: ACS Mater. Au 2024, 4, 604–611
Read Online

ACCESS | Metrics & More | Article Recommendations | Supporting Information

**ABSTRACT:** Moisture-sensitive fluorescent emitters are a class of smart materials that can change their emission behavior upon exposure to water. In this study, we have synthesized two highly fluorescent organic emitters, 4BPy-PTA and 2BPy-PTA, and showed how moisture sensitivity can be enhanced by molecular design modification. Owing to the different nitrogen atom positions in the acceptor units, the emitters show different degrees of moisture sensitivity. Upon moisture exposure, both emitters change their emission color from greenish-yellow to blue, but a larger shift was witnessed in 4BPy-PTA (81 nm) than in 2BPy-PTA (68 nm). Moisture exposure enhances the photoluminescence quantum yield (PLQY) of 4BPy-PTA from 37 to 48%, whereas it suppresses the PLQY of 2BPy-PTA from 59 to 15%. A shorter moisture sensing time, large emission color shift, and enhanced PLQY make 4BPy-PTA a better moisture-sensitive material than 2BPy-PTA. Interestingly, the emission colors of the emitters can be completely regained by heating and partially by applying mechanical force to the moisture-exposed solids. In addition, these emitters also show mechanochromic luminescence behavior with a completely reversible emission color switch between blue and green.

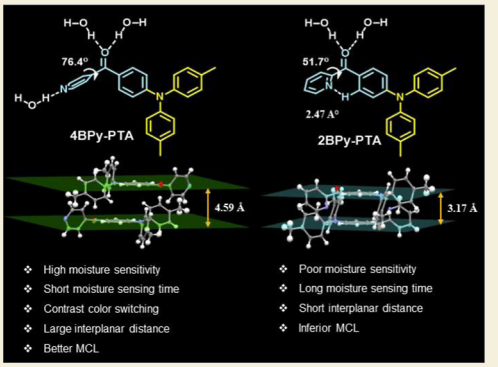


**KEYWORDS:** *moisture-sensitive emitters, relative humidity (RH), humidity sensor, mechanochromic luminescence (MCL), moisture induced crystallinity*

## INTRODUCTION

Relative humidity (RH) refers to the ratio between the moisture content present in the air at a particular temperature and the maximum moisture holding capacity of the air at that particular temperature.[1,2] RH is a relative quantity that indicates any kind of deviation in the moisture content of the surrounding air.[3] The abnormal moisture content has an adverse effect; hence, the accurate detection and regulation of moisture is one of the key aspects of various sectors, including health care,[4−7] manufacturing industries, agriculture, food packaging,[6,7] environmental monitoring, consumer electronics, and many more.[8−11] Currently, there are two kinds of moisture sensors, (1) electronic and (2) fluorescent. These sensors undergo changes in their properties (physical, chemical, or electrical) upon exposure to moisture. Electronic moisture sensors gather information by altering their electrical capacitance, resistance, and thermal conductance.[8,12] The fluorescent sensors are notably simpler, and their sensing can easily be noticed by the naked eye. In simple words, fluorescent moisture sensors are the smart luminescent materials that can detect the moisture and convey the information in the form of changing their photophysical properties, which includes the shifting of emission color, emission intensity, and luminescent nature of the material.[13−17] Though there are reports on organic fluorescent moisture sensing materials, there is still a lack of a molecular design strategy to enhance the moisture sensitivity.

The majority of the fluorescent emitters suffer from aggregation-caused quenching (ACQ) in their solid state.[18−20] To avoid this quenching, additional moieties are used that can minimize ACQ and enhance the emission intensity in the solid state. These additional moieties can be directly attached to the emitter by a covalent bond or can be used as secondary reagents to form multicomponent materials.[21−23] However, these additional groups complicate the synthesis and also affect the overall stability of multicomponent fluorescent materials.[24] Thus, designing an emitter with solid-state enhanced emission is highly praiseworthy. For an efficient fluorescent sensor, a contrast emission color

Received: May 13, 2024
Revised: August 19, 2024
Accepted: August 22, 2024
Published: September 4, 2024

**Scheme 1. Molecular Structure and Synthesis Procedure of 4BPy-PTA and 2BPy-PTA**

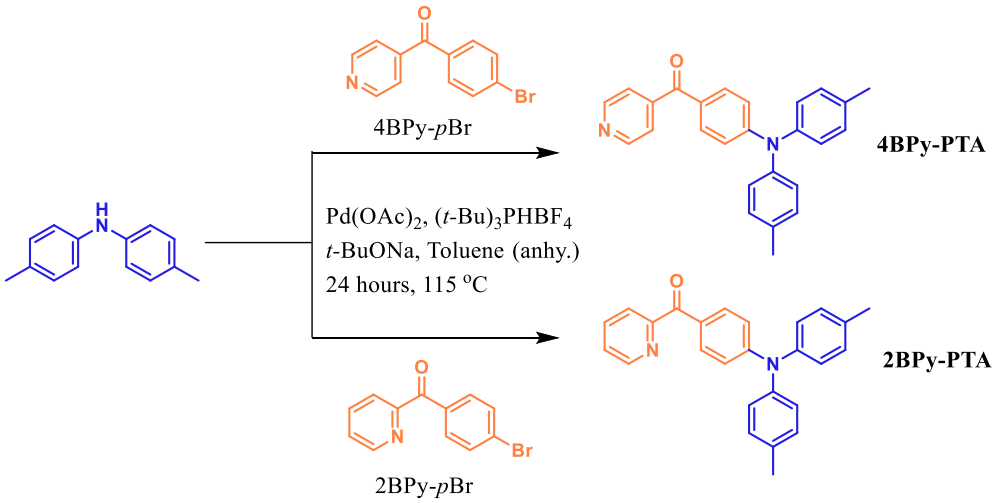


switching accompanied by an enhanced emission intensity is highly desired, which should be easily noticeable by the naked eye. However, a contrast emission color switching purely organic fluorescent moisture sensor is rare. In the case of fluorescent moisture sensors, the reversibility in their emission color after removing moisture is again very crucial; this ultimately decides the potential utility of that material.

Here, we have synthesized two simple organic donor−acceptor-based fluorescent isomers 2BPy-PTA and 4BPy-PTA, featuring a di-*p*-tolylamine donor and either 2-benzoylpyridine or 4-benzoylpyridine as an acceptor. Additionally, we investigated how moisture sensitivity can be enhanced by finetuning the molecular design. The twisted nature of the emitters helps in retaining a high photoluminescence quantum yield (PLQY) in their solid state, which is advantageous for various solid-state applications. Moisture exposure causes a blue shift in the emission spectra of the emitters, accompanied by a phase transition from amorphous to crystalline. 2BPy-PTA, which contains the 2-pyridine unit, exhibits low moisture sensitivity with an emission shift of 68 nm and requires 8 h of exposure. In contrast, 4BPy-PTA, having 4-pyridine units, demonstrates faster moisture sensitivity with a greater emission shift of 81 nm and enhanced PLQY. Moreover, both emitters show a good reversibility of their emission spectra after removal of moisture. The donor−acceptor architecture also helps in getting the mechanochromic luminescence (MCL) property; however, the different nitrogen position in the pyridine unit also controls their MCL behavior. We believe this study will provide fundamental insights into the molecular design of better organic emitters for moisture sensing and MCL.

## EXPERIMENTAL SECTION

### Synthesis of 4BPy-PTA

In a 100 mL cleaned and dried sealed tube, (4-bromophenyl)(pyridin-4-yl)methanone (4BPy-*p*Br) (2 g, 7.6 mmol), di-*p*-tolylamine (PTA) (1.5 g, 7.6 mmol), palladium acetate (0.085 g, 5 mol %), tri*tert*-butyl phosphine tetrafluoro borate (0.33 g, 1.14 mmol), and sodium *tert*-butoxide (1.5 g, 15 mmol) were taken. After evacuating air, the sealed tube was purged with nitrogen, and this process is repeated three times. Then, 40 mL of anhydrous toluene was added, and the reaction mixture was allowed to stir at 115 °C for 24 h. After completion of the reaction, toluene was removed under reduced pressure, and the product was extracted with ethyl acetate. The final organic part was concentrated under reduced pressure. The compound was purified by silica gel column chromatography using ethyl-acetate/*n*-hexane as eluent to afford yellow color (4-(di-*p*-tolylamino)phenyl)(pyridin-4-yl)methanone (4BPy-PTA) with 52% yield. $^1$H NMR (400 MHz, $CDCl_3$): $\delta$ 8.72 (d, $J$ = 6.0 Hz, 2H), 7.62 (d, $J$ = 8.9 Hz, 2H), 7.49 (d, $J$ = 6.0 Hz, 2H), 7.12 (d, $J$ = 8.0 Hz, 4H), 7.05 (d, $J$ = 8.4 Hz, 4H), 6.88 (d, $J$ = 9.0 Hz, 2H), 2.31 (s, 6H). $^{13}$C NMR (126 MHz, $CDCl_3$): $\delta$ 193.06, 153.15, 150.06, 145.90, 143.42, 135.12, 132.10, 130.39, 126.74, 126.40, 122.71, 117.83, 20.97. HRMS (ESI$^+$) calcd for $C_{26}H_{23}N_2O$ [M + H]$^+$, 379.1810; found, 379.1814.

### Synthesis of 2BPy-PTA

A procedure similar to 4BPy-PTA synthesis was followed for the synthesis of 2BPy-PTA. In a 100 mL cleaned and dried sealed tube, (4-bromophenyl)(pyridin-2-yl)methanone (2BPy-*p*Br) (2.5 g, 8.09 mmol), di-*p*-tolylamine (PTA) (1.6 g, 8.17 mmol), palladium acetate (0.09 g, 5 mol %), tri*tert*-butyl phosphine tetrafluoro borate (0.35 g, 1.21 mmol), and sodium *tert*-butoxide (1.55 g, 16.18 mmol) were taken. The compound was purified by silica gel column chromatography using ethyl-acetate/*n*-hexane as eluent to afford yellow color (4-(di-*p*-tolylamino)phenyl)(pyridin-2-yl)methanone (2BPy-PTA) with 60% yield. $^1$H NMR (400 MHz, $CDCl_3$): $\delta$ 8.65 (d, $J$ = 4.0 Hz, 1H), 7.94−7.90 (m, 3H), 7.83 (td, $J$ = 7.7, 1.8 Hz, 1H), 7.40 (ddd, $J$ = 7.5, 4.8, 1.3 Hz, 1H), 7.10 (d, $J$ = 8.0 Hz, 4H), 7.04 (d, $J$ = 8.5 Hz, 4H), 6.91 (d, $J$ = 9.0 Hz, 2H), 2.31 (s, 6H). $^{13}$C NMR (126 MHz, $CDCl_3$): $\delta$ 191.73, 156.29, 152.63, 148.23, 143.83, 136.96, 134.59, 132.88, 130.24, 127.47, 126.25, 125.55, 124.46, 118.23, 20.96. HRMS (ESI$^+$) calcd for $C_{26}H_{23}N_2O$ [M + H]$^+$, 379.1810; found, 379.1816.

### Synthesis of BP-PTA

Above synthesis procedure was followed to prepare BP-PTA. In a 100 mL cleaned and dried sealed tube, (4-bromophenyl)(phenyl)-methanone (BP-*p*Br) (0.5 g, 1.91 mmol), di-*p*-tolylamine (PTA (0.38 g, 1.93 mmol), palladium acetate (0.04 g, 10 mol %), tri*tert*-butyl phosphine tetrafluoro borate (0.08 g, 0.28 mmol), and sodium *tert*-butoxide (0.36 g, 3.82 mmol) were taken. The compound was purified by silica gel column chromatography using ethyl-acetate/*n*-hexane as the eluent to afford yellow color (4-(di-*p*-tolylamino)-phenyl)(phenyl)methanone (BP-PTA) with 55% yield. $^1$H NMR (500 MHz, $CDCl_3$): $\delta$ 7.73 (d, $J$ = 7.9 Hz, 2H), 7.66 (d, $J$ = 8.5 Hz, 2H), 7.53−7.48 (m, 1H), 7.42 (t, $J$ = 7.6 Hz, 2H), 7.13−7.04 (m, 8H), 6.92 (d, $J$ = 8.5 Hz, 2H), 2.32 (s, 6H). $^{13}$C NMR (126 MHz, $CDCl_3$): $\delta$ 152.33, 143.89, 138.70, 134.57, 132.03, 131.56, 130.28, 129.62, 128.66, 128.10, 126.16, 118.33, 20.96. HRMS (ESI$^+$) calcd for $C_{27}H_{24}NO$ [M + H]$^+$, 378.1858; found, 378.1855.



https://doi.org/10.1021/acsmaterialsau.4c00036
ACS Mater. Au 2024, 4, 604−611

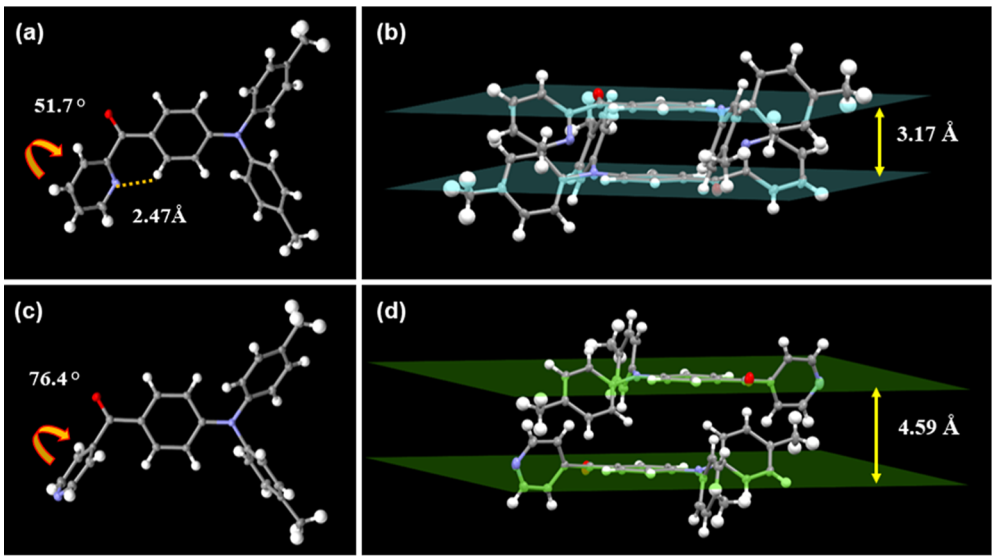


**Figure 1.** Single crystal structure of (a) 2BP-PTA and (c) 4BPy-PTA showing the dihedral angle between the pyridine unit and central benzene ring; interplanar distance of (b) 2BPy-PTA and (d) 4BPy-PTA obtained from single crystal XRD. [Color code; gray = carbon; white = hydrogen; blue = nitrogen; and red = oxygen].

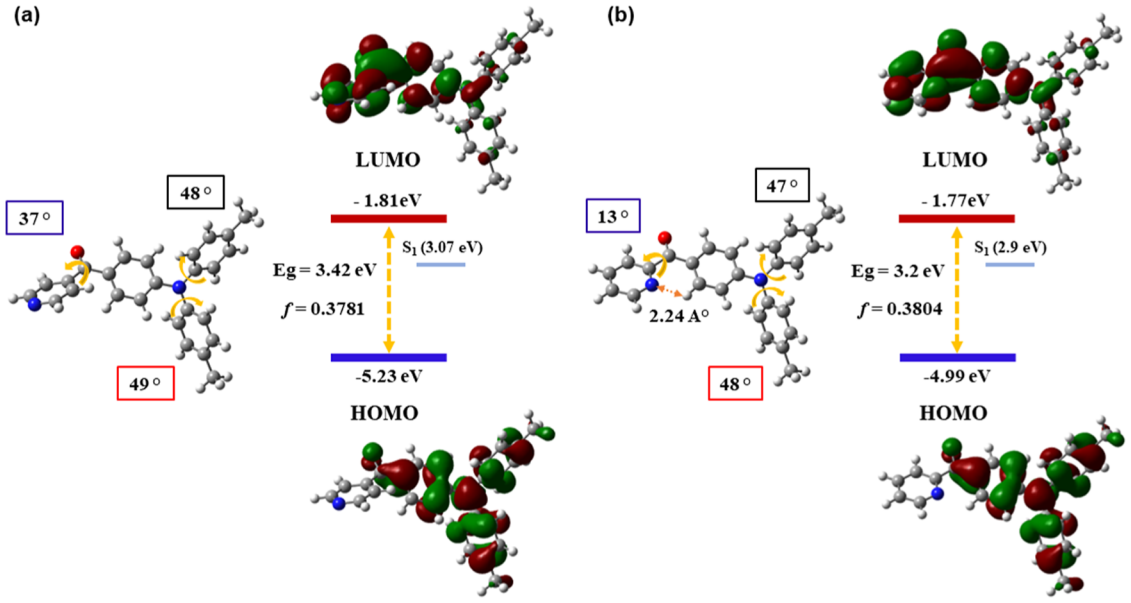


**Figure 2.** Optimized molecular structures, dihedral angle between pyridine and central benzene ring, HOMO-LUMO distribution, and $S_1$ energy levels and optical band gaps of (a) 4BPy-PTA and (b) 2BPy-PTA evaluated from TD-DFT using the B3LYP 6-311G(d,p) basis set.

## RESULTS AND DISCUSSION

### Molecular Structure and Single Crystal XRD Analysis

Molecular structures and synthesis routes of (4-(di-*p*-tolylamino)phenyl)(pyridin-4-yl)methanone (4BPy-PTA) and (4-(di-*p*-tolylamino)phenyl)(pyridin-2-yl)methanone (2BPy-PTA) are shown in Scheme 1. Both emitters comprise a donor−acceptor architecture where 4-benzoylpyridines or 2-benzoylpyridines (4BPy or 2BPy) act as acceptors and di-*p*-tolylamine (PTA) as the donor. The emitters were synthesized in two steps: first, the preparation of intermediates, followed by the Buchwald−Hartwig amination coupling of intermediates with the donor unit to obtain the final product.[25] The detailed synthesis procedures and structural characterizations of the emitters are provided in the Experimental Section and in the Supporting Information.

To understand molecular packing, single crystal X-ray analysis was performed for 4BPy-PTA and 2BPy-PTA (Figure 1). Both crystals have monoclinic unit cells and were grown by solution growth technique in an acetone/methanol solvent mixture (Tables S1 and S2). In the crystal structure, neighboring molecules are arranged in a head-to-tail alignment, wherein the pyridine units, keto groups, and the central benzene rings are engaged in multiple C−H···N, CO···H, C−H···$\pi$, and $\pi$···$\pi$ stacking interactions (Figures S2 and S4). In 2BPy-PTA, the 2-pyridine unit results in a strong intramolecular N···H−C interaction with a distance of 2.47 Å. This intramolecular interaction decreases the dihedral angle of the acceptor unit (51.7°) and reduces the interplanar distance in the 2BPy-PTA crystal (Figure 1a,b). Whereas, the lack of such a strong intramolecular N···H−C interaction in 4BPy-PTA


https://doi.org/10.1021/acsmaterialsau.4c00036
ACS Mater. Au 2024, 4, 604−611

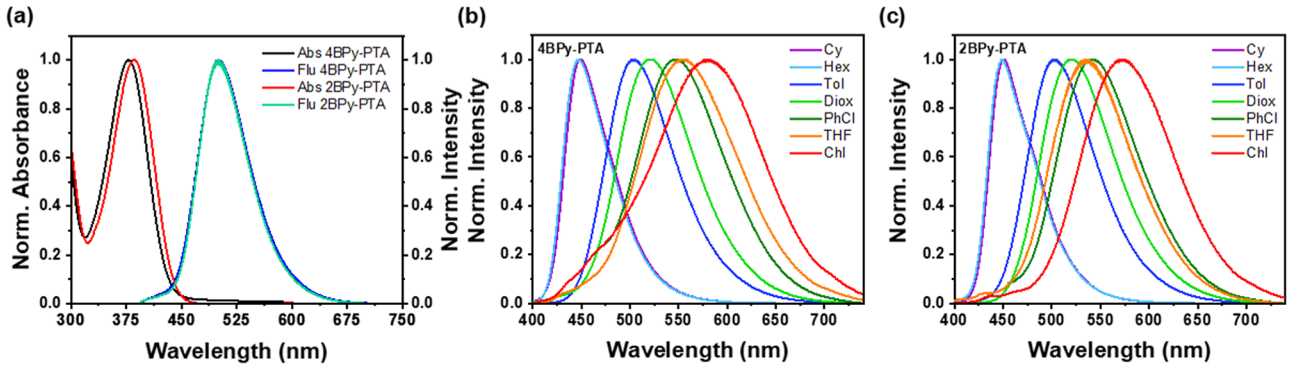


**Figure 3.** (a) Normalized UV−visible absorbance and PL measurements of 4BPy-PTA and 2BPy-PTA in 0.01 mM toluene solution, $\lambda_{ex}$ = 380 nm; solvatochromic study of (b) 4BPy-PTA and (c) 2BPy-PTA in cyclohexane, hexane, toluene, 1,4-dioxane, chlorobenzene, tetrahydrofuran, and chloroform solutions.

**Table 1. Photophysical Properties of 4BPy-PTA and 2BPy-PTA**

| emitter | $\lambda_{abs}$ (nm)[a] | $\lambda_{em}$ (nm)[b] | HOMO/LUMO (eV)[c] | $E_g$ (eV)[d] | $S_1$ (eV)[e] | $\tau_p$ (ns) (Tol)[f] | PLQY (%) (Tol/film)[g] | $T_d$ (°C)[h] |
|---|---|---|---|---|---|---|---|---|
| 4BPy-PTA | 290, 379 | 500 | −5.38/−2.54 | 2.84 | 2.80 | 4.12 | 19/33 | 292 |
| 2BPy-PTA | 290, 386 | 500 | −5.34/−2.53 | 2.81 | 2.81 | 4.68 | 24/48 | 307 |

[a]Absorbance of 4BPy-PTA and 2BPy-PTA in toluene solution. [b]Emission maxima of emitters in toluene solution. [c]Experimental HOMO and LUMO values evaluated from CV. [d]Experimental bandgap of the emitters calculated from the onsets of the UV−visible absorption spectra. [e]Experimental singlet energy level evaluated from the onset of fluorescence spectra. [f]Prompt lifetime of the materials in toluene solution. [g]PLQY in toluene solution and in neat film. [h]Decomposition temperature with 5 wt % loss of the compound measured from thermogravimetric analysis under a nitrogen environment.

results in a large dihedral angle (76.4°) and an extended interplanar $\pi\cdots\pi$ stacking distance (4.59 Å) (Figure 1c,d).

## Density Functional Theory Calculations

To get more insight into the frontier molecular orbital (FMO) distribution and energy level alignments, time-dependent density functional theory (TD-DFT) calculations were performed for 4BPy-PTA and 2BPy-PTA using the B3LYP, 6-311G(d,p) basis set (Figure 2). Energy levels were calculated using the optimized molecular geometry. The theoretical calculations show the distribution of highest occupied molecular orbitals (HOMOs) on *p*-tolylamine and lowest unoccupied molecular orbitals (LUMOs) on benzoylpyridine units. The separation of FMOs suggests the charge transfer (CT) nature of the emitters.[26] However, both 4BPy-PTA and 2BPy-PTA show significant FMO overlaps, resulting in enhanced oscillator strength (*f*).[27] DFT calculations also show that both emitters have nearly identical LUMO but slightly different HOMO energy levels (Table S3). 2BPy-PTA has a shallower HOMO energy level than 4BPy-PTA. The 2-pyridine unit brings partial planarity in 2BPy-PTA, which increases the conjugation, leading to a shallower HOMO energy level.[28]

## Photophysical Properties

UV−visible absorptions of 4BPy-PTA and 2BPy-PTA were measured in toluene solution (0.01 mM) shown in Figure 3, and the data are summarized in Table 1. The absorption spectra of the emitters have two broad bands, with a peak at 290 nm dedicated to $\pi-\pi^*$ transitions. The absorption spectra of 4BPy-PTA and 2BPy-PTA at low energy regions of 379 and 386 nm, respectively, are due to the intramolecular charge transfer (ICT) transitions between the *p*-tolylamine donor and the benzoylpyridine acceptor.[26] A slightly bathochromic shift of the ICT band in 2BPy-PTA indicates the presence of better conjugation in the molecule than in 4BPy-PTA.[29,30] As it is evident from the DFT calculations, the position of the "N" atom makes the 2BPy-PTA acceptor planar and hence a better $\pi$ conjugation.

The photoluminescence (PL) measurements of 4BPy-PTA and 2BPy-PTA were done in toluene solution (0.01 mM) using an excitation wavelength of 380 nm (Figure 3), and their corresponding values are given in Table 1. The toluene solutions of 4BPy-PTA and 2BPy-PTA show intense green emissions with $\lambda_{max}$ values at 500 nm. From the onsets of the PL spectra, singlet excited energy levels ($S_1$) of 4BPy-PTA and 2BPy-PTA were calculated to be 2.80 and 2.81 eV, respectively. The emission spectra of both emitters are structureless in appearance, indicating the CT nature of the singlet excited states.[31,32] To further confirm the charge-transfer nature of the $S_1$ state, PL measurements of the emitters were recorded in different solvents (0.01 mM) with varying polarities (Figure 3b,c), and both emitters show positive solvatochromism. In nonpolar cyclohexane solutions, 4BPy-PTA and 2BPy-PTA show intense blue emissions with $\lambda_{max}$ at 448 and 449 nm, respectively (Table S4). With increasing the solvent polarity, the emission peaks of the emitters start shifting toward longer wavelengths. In highly polar chloroform solutions, 4BPy-PTA and 2BPy-PTA exhibit broad and significantly red-shifted emissions, with $\lambda_{max}$ at 580 and 571 nm, respectively (Figure 3 and Table S4). In polar media, the CT excited state of the emitters stabilized due to the high dipole moment of the solvents, leading to a broad and red-shifted emission peak accompanied by quenched emission.[26,33,34] The presence of this solvatochromic shift confirms the ICT nature of the emitters, which arises from their donor−acceptor molecular architecture.[35]

Relative PLQY of the emitters was measured in toluene using ethanol solution of 9,10-diphenyl anthracene as a reference (Figure S5).[36−38] The solution PLQYs of 4BPy-PTA and 2BPy-PTA were found to be 19 and 24%,


https://doi.org/10.1021/acsmaterialsau.4c00036
ACS Mater. Au 2024, 4, 604−611

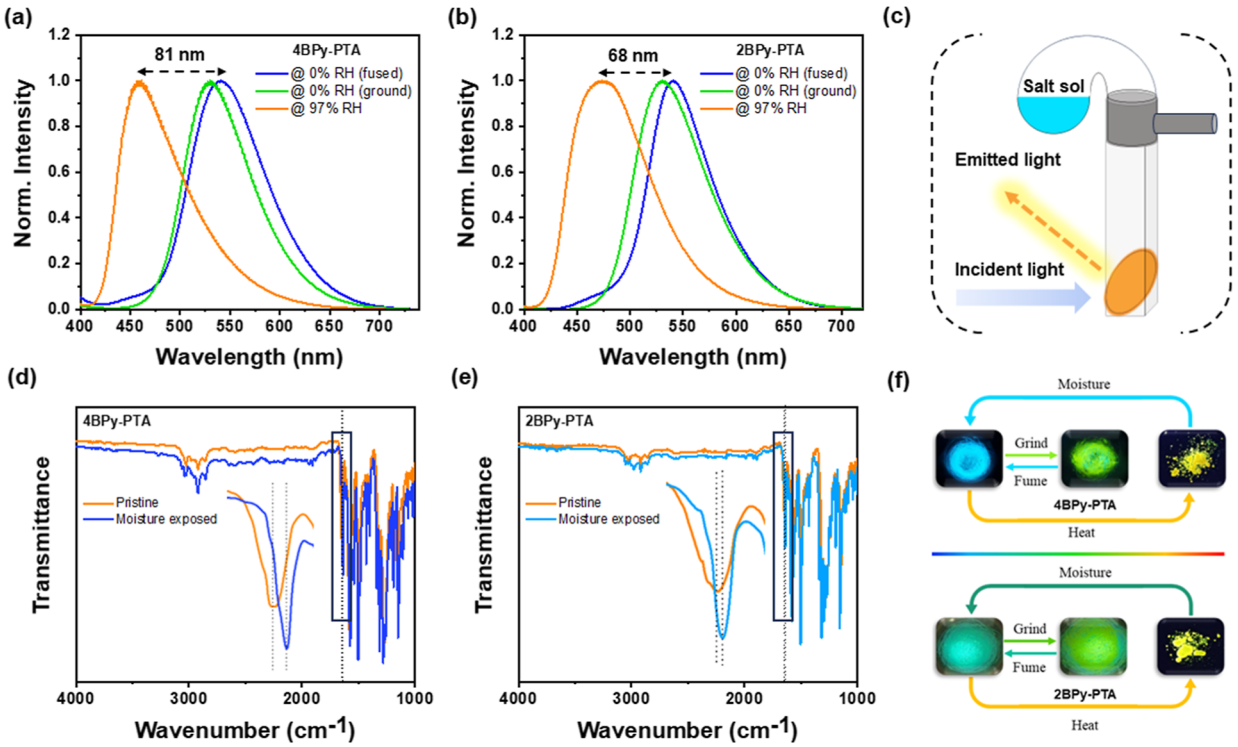


**Figure 4.** (a) Moisture sensing study of 4BPy-PTA; (b) moisture sensing study of 2BPy-PTA; (c) schematic representation of moisture sensing set up; (d) FTIR of pristine and moisture exposed solids of 4BPy-PTA; (e) FTIR of pristine and moisture exposed solids of 2BPy-PTA; (f) digital photographs showing the emission colors of pristine solids, moisture exposed solids, and ground forms of 4BPy-PTA and 2BPy-PTA.

respectively (Table 1). However, these emitters show the enhanced PLQY in thin film, and 4BPy-PTA and 2BPy-PTA shows quantum yields of 33 and 48%, respectively (Figure S6). Both emitters are giving higher PLQYs in their solid state than in solution. This higher quantum yield in solid state is due to restrictions on nonradiative decay channels, which is commonly known as solid state enhanced emission.[18,39] The high PLQY of 2BPy-PTA in its thin film suggests that the emitter is properly suppressing the nonradiative decay channels. To check the thermal stability of the emitters, thermogravimetric analyses (TGA) were done under an nitrogen atmosphere (Figure S7). The degradation temperature ($T_d$) of 4BPy-PTA with 5% weight loss was found to be 292 °C, while for 2BPy-PTA, it is a little higher (307 °C). The higher degradation temperature of 2BPy-PTA is possibly due to higher rigidity caused by strong intramolecular N···H−C interactions within the acceptor unit.

## Moisture Sensing

The moisture sensing behavior of the emitters was explored with their sublime solids or pristine forms. The emitters were exposed to moisture, and the change in their fluorescence emission behavior was carefully monitored. The moisture sensing set up is shown in Figure 4c.[40] The sublimed solids of the emitters look yellow with a glassy and transparent appearance, giving emission at 541 nm (Figure 4 and Table S5). After moisture exposure, the emission colors of the emitters blue-shifted to 460 nm in 4BPy-PTA and 473 nm in 2BPy-PTA (Figure 4a,b). However, in the sublimed solids, molecules are random and tightly packed, thus showing slow moisture sensing (more than 8 h). Therefore, ground solids (1 mg) of the sublimed form were used for the sensing experiment. The ground solids of the emitters show green emission with a $\lambda_{max}$ of 530 nm. 4BPy-PTA showed blue-shifted emission within 2 h of the moisture exposure, while 2BPy-PTA takes 8 h to change its emission color. It is clear that irrespective of the forms of emitter used (sublimed or ground), the final blue-shifted emission colors remain the same (460 in 4BPy-PTA and 473 in 2BPy-PTA). To understand the effect of different RH levels on the emission color shift, the emitter (4BPy-PTA) was exposed to different RH levels (11, 43, and 97%), and PL emission was carefully monitored (Figure S8). The sample exposed to 97% RH completely switches its emission color from green to blue after 2 h, while the sample exposed to 11% RH is still in the green region with a small hump at ∼460 nm. The sample exposed to lower RH takes a longer time but ultimately shows blue emission. Here, the blue and green emission regions represent hydrated and anhydrate emitters, respectively. This experiment indicates that water coordination with the emitter can happen at any RH level, and the final emission color will always remain the same. However, the moisture exposure time to completely shift the emission color depends on RH level. To get a relationship between exposure time vs emission color, the PL spectra of 4BPy-PTA were recorded with a time interval of 10 min by exposing an RH of 97%. The CIE values are linearly changing from the green [0.31, 0.57] to blue region [0.18, 0.25] (Figure S9).

To quantify the change in emission intensity during moisture sensing, the absolute PLQY of the emitters in their different forms was recorded. After moisture exposure, 4BPy-PTA witnessed an enhanced PLQY from 37 to 48%, whereas 2BPy-PTA showed a drastic reduction in its PLQY from 59 to 15%. This contrasting behavior is possibly because of their difference in pyridine nitrogen position. In the sublimed solids, molecules were random and tightly packed; this close proximity of emitters led to the lower PLQY in the fused


https://doi.org/10.1021/acsmaterialsau.4c00036
ACS Mater. Au 2024, 4, 604−611

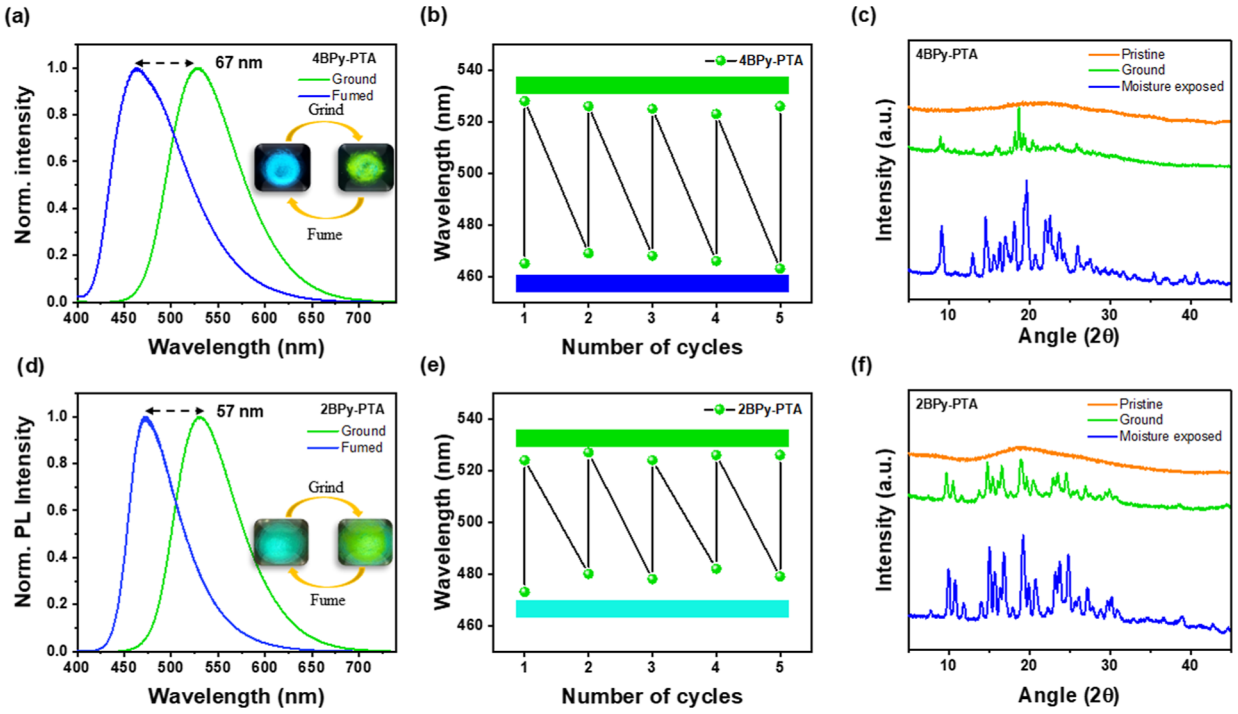


**Figure 5.** (a) MCL study of 4BPy-PTA; (b) reversible switching of emission color in 4BPy-PTA during MCL study; (c) powder XRDs of different solids of 4BPy-PTA obtained during the MCL experiment; (d) MCL study of 2BPy-PTA; (e) reversible switching of emission color in 2BPy-PTA during MCL study; (f) powder XRDs of different solids of 2BPy-PTA obtained during the MCL experiment.

state of 4BPy-PTA.[18,19,41] The coordination of water with emitters possibly increases the intermolecular distance, resulting in a higher PLQY in moisture-exposed 4BPy-PTA. In contrast, 2BPy-PTA shows higher PLQY in its fused state than the moisture-exposed form because of the better solid-state enhanced emission behavior.

From the above experiments, it is clear that the pyridine nitrogen position has a great role in improving the moisture sensitivity of an organic material. Previous studies claim the noncovalent interaction, particularly H-bonding between the emitter and water molecule, is primarily responsible for the moisture sensing behavior of an emitter.[16,17] In our emitters, we have two coordinating groups, keto and pyridine, and the only structural difference between 4BPy-PTA and 2BPy-PTA is the position of nitrogen in pyridine. Hence, appropriate nitrogen atom positioning acceptor units are crucial for enhancing moisture sensitivity. To understand the actual role of the nitrogen atom on the sensing mechanism, single-crystal XRDs were done for these emitters.

Single crystal analysis confirms the presence of a strong intramolecular N···H−C interaction in 2BPy-PTA (wide supra). This intramolecular interaction restricts the co-ordination of water with 2-pyridine units in 2BPy-PTA. Thus, only the keto group can interact with water in 2BPy-PTA. As the water coordination tendency of pyridine is greater than the keto group, 2BPy-PTA takes longer time to sense moisture.[42] To confirm the active role of pyridine and ketone, the moisture sensitivity of BP-PTA was studied. BP-PTA is structurally similar to our emitters but without nitrogen on the acceptor unit (Scheme S3). Pristine BP-PTA shows blue-green emission (493 nm), which shifts its $\lambda_{max}$ to the blue region (443 nm) after moisture exposure (Figure S10 and Table S5). Interestingly, both BP-PTA and 2BPy-PTA take nearly the same amount of time to sense moisture. This result clearly shows that the C═O group is primary responsible for the moisture sensing in 2BPy-PTA. On the other hand, 4BPy-PTA has two coordinating groups (keto and pyridine), which are free to interact with water; therefore, the emitter shows a shorter moisture sensing time and shows a larger $\Delta\lambda$. The keto group's involvement in moisture sensing was checked by recording FTIR of 4BPy-PTA and 2BPy-PTA in their pristine and moisture exposed forms (Figure 4d,e). The pristine forms of 4BPy-PTA and 2BPy-PTA show a C═O stretching frequency at 1649 and 1645 $cm^{-1}$, which after moisture exposure shift to 1639 and 1642 $cm^{-1}$, respectively. The shift in the C═O stretching frequency confirms the water coordination (H-bonding) with the keto group.[43]

## Mechanochromic Luminescence

The original emission color and phase of the moisture exposed materials can be reverted by applying thermal stimuli (heating) or mechanical stimuli (grinding; Figure 5). Thermal stimuli remove the coordinated water molecules and thus revert the emission color. However, mechanical force displaces the crystal planes, causing a change in their emission peak. Grinding leads to the deformation in the packing of molecules in the system, which directly affects the donating or accepting strengths of the donor (D) or acceptor (A) units in D−A-based emitters.[26,44] The variation in the strengths of donor or acceptor units leads to the change in the energy levels, which ultimately pamper the emission color.[45,46] From the X-ray analysis, it is clear that 2BPy-PTA has a shorter interplanar distance as compared to 4BPy-PTA (Figure 1). As a result, 2BPy-PTA exhibits a smaller $\lambda_{max}$ shift from 473 to 530 nm (Figure 5d and Table S5). On the other hand, a large interplanar distance in 4BPy-PTA allows it to easily get distorted by mechanical force. Therefore, after grinding, 4BPy-PTA shows a larger emission wavelength shift from 460 to 530 nm than 2BPy-PTA (Figure 5a).


https://doi.org/10.1021/acsmaterialsau.4c00036
ACS Mater. Au 2024, 4, 604−611

The reversibility of the emission can be achieved by external stimuli such as DCM fuming, water exposure, or heat. Both emitters show complete reversibility up to 5 cycles, as demonstrated in Figure 5b,e. As already discussed, the moisture exposed solids are crystalline in nature, and by grinding, they partly lose their crystallinity, which is confirmed from the weak p-XRD peaks (Figure 5c,f). On the other hand, by heating the emitter, they completely change their morphology to amorphous and acquire their original greenish-yellow emission color ($\lambda_{max}$ = 541 nm).

## CONCLUSIONS

Here, we have designed two simple organic fluorescent isomers, 4BPy-PTA and 2BPy-PTA, and showed the active role of the pyridine "N" atom position in enhancing the moisture sensitivity. Theoretical calculations and photophysical studies confirm the CT nature of the emitters. 2BPy-PTA contains 2-benzoyl pyrdine acceptor unit, which forms a strong intramolecular N···H−C interaction and blocks water coordination. The other isomer, 4BPy-PTA, lacks such intramolecular interaction, hence allowing easy water molecule coordination. Therefore, 4BPy-PTA shows high contrast emission color switching from 541 to 460 nm, enhanced emission intensity (PLQY increases from 37 to 48%), and a short moisture exposure time (2 h). While 2BPy-PTA needs a longer exposure time (8 h) to change its emission from 541 to 473 nm, and PLQY also reduced from 59 to 15% upon moisture exposure. Additionally, both emitters show MCL behavior, but the extent of MCL behaviors is also affected by nitrogen position. Hence, changing the nitrogen position leads to a drastic impact on the moisture sensitivity of an emitter. We anticipate that this research will provide valuable insights into the development of superior organic emitters for moisture or humidity sensing applications.

## ASSOCIATED CONTENT

### Supporting Information

The Supporting Information is available free of charge at https://pubs.acs.org/doi/10.1021/acsmaterialsau.4c00036.

Detailed synthesis procedures, characterizations (NMR and HRMS), single crystal XRDs, PLQY, BP-PTA photophysical data, and TGA (PDF)

## AUTHOR INFORMATION


### Corresponding Author

**Pachaiyappan Rajamalli** − *Materials Research Centre, Indian Institute of Science, Bangalore 560012, India;* orcid.org/0000-0001-8079-0425; Email: rajamalli@iisc.ac.in

### Authors

**Gyana Prakash Nanda** − *Materials Research Centre, Indian Institute of Science, Bangalore 560012, India;* orcid.org/0000-0002-4592-5758

**Rajan Suraksha** − *Materials Research Centre, Indian Institute of Science, Bangalore 560012, India*

Complete contact information is available at: https://pubs.acs.org/10.1021/acsmaterialsau.4c00036


### Author Contributions

The emitters were synthesized by Gyana and Suraksha. All the photophysical studies, moisture sensing studies, mechanochromic studies, and XRD-analysis were done by Gyana. The data analysis was done by Gyana and Rajamalli. The manuscript was written by Gyana under the guidance of Rajamalli. CRediT: **Gyana Prakash Nanda** conceptualization, data curation, formal analysis, methodology, writing - original draft; **Rajan Suraksha** data curation, formal analysis; **Pachaiyappan Rajamalli** conceptualization, funding acquisition, project administration, resources, supervision, writing - review & editing.

### Notes

The authors declare no competing financial interest.

## ACKNOWLEDGMENTS

G.P.N. thanks the Council of Scientific & Industrial Research (CSIR), India, for the Senior Research Fellowship (SRF). P.R. thanks the Indian Institute of Science (IISc) and the Science & Engineering Research Board (SERB), India, for the SERB-Power Grant (SPG) (grant no: SPG/2020/000107), Rekha Rao Young Investigator award, and IGSTC WISER award for financial support. The authors are grateful to the Department of Science and Technology (DSTFIST: SR/FST/PSII009/2010) for the instrumental facilities at MRC and IISc for X-ray and NMR facilities.

## REFERENCES


(1) Tiefenbacher, K. F. Chapter Ten—Glossary of Terms in Wafers, Waffles and Adjuncts. In *The Technology of Wafers and Waffles II*; Tiefenbacher, K. F., Ed.; Academic Press, 2019; pp 325−411.

(2) Patel, G.; Prudhvi, P. V. V. P.; Patra, A.; Pathak, S. S.; Sonawane, A. D.; Shirkole, S. S. 20—Different parameters affecting the efficiency of dryers. In *Drying Technology in Food Processing*; Jafari, S. M., Malekjani, N., Eds.; Woodhead Publishing, 2023; pp 705−742.

(3) Farahani, H.; Wagiran, R.; Hamidon, M. N. Humidity sensors principle, mechanism, and fabrication technologies: a comprehensive review. *Sensors* **2014**, *14* (5), 7881−7939.

(4) Scott, C.; Cameron, S.; Cundell, J.; Mathur, A.; Davis, J. Adapting resistive sensors for monitoring moisture in smart wound dressings. *Curr. Opin. Electrochem.* **2020**, *23*, 31−35.

(5) Liang, Y.; Ding, Q.; Wang, H.; Wu, Z.; Li, J.; Li, Z.; Tao, K.; Gui, X.; Wu, J. Humidity Sensing of Stretchable and Transparent Hydrogel Films for Wireless Respiration Monitoring. *Nano-Micro Lett.* **2022**, *14* (1), 183.

(6) Yousefi, H.; Su, H.-M.; Imani, S. M.; Alkhaldi, K.; M Filipe, C. D.; Didar, T. F. Intelligent Food Packaging: A Review of Smart Sensing Technologies for Monitoring Food Quality. *ACS Sens.* **2019**, *4* (4), 808−821.

(7) Dodero, A.; Escher, A.; Bertucci, S.; Castellano, M.; Lova, P. Intelligent Packaging for Real-Time Monitoring of Food-Quality: Current and Future Developments. *Appl. Sci.* **2021**, *11*, 3532.

(8) Arman Kuzubasoglu, B. Recent Studies on the Humidity Sensor: A Mini Review. *ACS Appl. Electron. Mater.* **2022**, *4* (10), 4797−4807.

(9) Delipinar, T.; Shafique, A.; Gohar, M. S.; Yapici, M. K. Fabrication and Materials Integration of Flexible Humidity Sensors for Emerging Applications. *ACS Omega* **2021**, *6* (13), 8744−8753.

(10) Chen, X.; Li, Y.; Wang, X.; Yu, H. Origami Paper-Based Stretchable Humidity Sensor for Textile-Attachable Wearable Electronics. *ACS Appl. Mater. Interfaces* **2022**, *14* (31), 36227−36237.

(11) Moustafa, H.; Morsy, M.; Ateia, M. A.; Abdel-Haleem, F. M. Ultrafast response humidity sensors based on polyvinyl chloride/graphene oxide nanocomposites for intelligent food packaging. *Sens. Actuators, A* **2021**, *331*, 112918.

(12) Ma, Z.; Fei, T.; Zhang, T. An overview: Sensors for low humidity detection. *Sens. Actuators, B* **2023**, *376*, 133039.

(13) Kumar, P.; Kaushik, R.; Ghosh, A.; Jose, D. A. Detection of Moisture by Fluorescent OFF-ON Sensor in Organic Solvents and Raw Food Products. *Anal. Chem.* **2016**, *88* (23), 11314−11318.

(14) Xu, W.; Li, F.; Cai, Z.; Wang, Y.; Luo, F.; Chen, X. An ultrasensitive and reversible fluorescence sensor of humidity using perovskite CH3NH3PbBr3. *J. Mater. Chem. C* **2016**, *4* (41), 9651−9655.
(15) Wang, T.; Wu, Y.; Xia, Y.; Yuan, Y.; Dou, Z.; Kan, C.; Zhang, N. Fluorescent and ratiometric humidity sensor based on cyano-substituted oligo(p-phenylene)/silica gel hybrid materials. *Dyes Pigm.* **2024**, *222*, 111862.
(16) Zhan, L.; Tang, Y.; Ning, W.; Xie, G.; Zhong, C.; Gong, S.; Yang, C. Humidity visualization through a simple thermally activated delayed fluorescent emitter: The role of hydrogen bonding. *Chem. Eng. J.* **2023**, *454*, 140182.
(17) Mamada, M.; Katagiri, H.; Adachi, C. Effect of Hydrogen Bonding on Thermally Activated Delayed Fluorescence Behaviors Based on a Study of Hydrate Crystals. *J. Phys. Chem. Lett.* **2023**, *14* (22), 5221−5225.
(18) Luo, J.; Xie, Z.; Lam, J. W. Y.; Cheng, L.; Tang, B. Z.; Chen, H.; Qiu, C.; Kwok, H. S.; Zhan, X.; Liu, Y.; Zhu, D. Aggregation-induced emission of 1-methyl-1,2,3,4,5-pentaphenylsilole. *Chem. Commun.* **2001**, No. 18, 1740−1741.
(19) Hong, Y.; Lam, J. W. Y.; Tang, B. Z. Aggregation-induced emission: phenomenon, mechanism and applications. *Chem. Commun.* **2009**, No. 29, 4332−4353.
(20) Nie, H.; Hu, K.; Cai, Y.; Peng, Q.; Zhao, Z.; Hu, R.; Chen, J.; Su, S.-J.; Qin, A.; Tang, B. Z. Tetraphenylfuran: aggregation-induced emission or aggregation-caused quenching? *Mater. Chem. Front.* **2017**, *1* (6), 1125−1129.
(21) Cheng, Y.; Wang, J.; Qiu, Z.; Zheng, X.; Leung, N. L. C.; Lam, J. W. Y.; Tang, B. Z. Multiscale Humidity Visualization by Environmentally Sensitive Fluorescent Molecular Rotors. *Adv. Mater.* **2017**, *29* (46), 1703900.
(22) Lan, R.; Gao, Y.; Shen, C.; Huang, R.; Bao, J.; Zhang, Z.; Wang, Q.; Zhang, L.; Yang, H. Humidity-Responsive Liquid Crystalline Network Actuator Showing Synergistic Fluorescence Color Change Enabled by Aggregation Induced Emission Luminogen. *Adv. Funct. Mater.* **2021**, *31* (17), 2010578.
(23) Sun, Q.; Qiu, X.; Lu, Y.; Xu, X.; Wang, H.; Xue, S.; Yang, W. AIE-active 9,10-bis(alkylarylvinyl)anthracences with pendent diethoxylphosphorylmethyl groups as solution-processable efficient EL luminophores. *J. Mater. Chem. C* **2017**, *5* (35), 9157−9164.
(24) Dong, Y. Q.; Lam, J. W. Y.; Tang, B. Z. Mechanochromic Luminescence of Aggregation-Induced Emission Luminogens. *J. Phys. Chem. Lett.* **2015**, *6* (17), 3429−3436.
(25) Forero-Cortés, P. A.; Haydl, A. M. The 25th Anniversary of the Buchwald−Hartwig Amination: Development, Applications, and Outlook. *Org. Process Res. Dev.* **2019**, *23* (8), 1478−1483.
(26) Deori, U.; Ravindran, E.; Nanda, G. P.; Ramanath, S. G.; Acharya, U.; Gandeepan, P.; Rajamalli, P. Design Strategy for Enabling Multifunctional Properties of Anthracene-based Emitters. *Chem.—Asian J.* **2023**, *18* (14), No. e202300352.
(27) Zeng, W.; Gong, S.; Zhong, C.; Yang, C. Prediction of Oscillator Strength and Transition Dipole Moments with the Nuclear Ensemble Approach for Thermally Activated Delayed Fluorescence Emitters. *J. Phys. Chem. C* **2019**, *123* (15), 10081−10086.
(28) Pavia, D. L.; Lampman, G. M.; Kriz, G. S.; Vyvyan, J. A. *Introduction to Spectroscopy*; Cengage Learning, 2014.
(29) Iwanaga, T.; Ogawa, M.; Yamauchi, T.; Toyota, S. Intramolecular Charge-Transfer Interaction of Donor−Acceptor−Donor Arrays Based on Anthracene Bisimide. *J. Org. Chem.* **2016**, *81* (10), 4076−4080.
(30) Kumar, S.; Rajamalli, P.; Cordes, D. B.; Slawin, A. M. Z.; Zysman-Colman, E. Highly Fluorescent Emitters Based on Triphenylamine-$\pi$-Triazine (D-$\pi$-A) System: Effect of Extended Conjugation on Singlet-Triplet Energy Gap. *Asian J. Org. Chem.* **2020**, *9* (9), 1277−1285.
(31) Uoyama, H.; Goushi, K.; Shizu, K.; Nomura, H.; Adachi, C. Highly efficient organic light-emitting diodes from delayed fluorescence. *Nature* **2012**, *492* (7428), 234−238.
(32) Pandey, N.; Tewari, N.; Pant, S.; Mehata, M. S. Solvatochromism and estimation of ground and excited state dipole moments of 6-aminoquinoline. *Spectrochim. Acta, Part A* **2022**, *267*, 120498.
(33) Reichardt, C. J. C. R. Solvatochromic Dyes as Solvent Polarity Indicators. *Chem. Rev.* **1994**, *94*, 2319−2358.
(34) Nigam, S.; Rutan, S. Principles and Applications of Solvatochromism. *Appl. Spectrosc.* **2001**, *55*, 362−370A.
(35) Kumari, R.; Varghese, A.; George, L.; Y N, S. Effect of solvent polarity on the photophysical properties of chalcone derivatives. *RSC Adv.* **2017**, *7* (39), 24204−24214.
(36) Brouwer, A. M. Standards for photoluminescence quantum yield measurements in solution. *IUPAC Technical Report*, 2011; Vol. *83*, pp 2213−2228.
(37) Morris, J. V.; Mahaney, M. A.; Huber, J. R. Fluorescence quantum yield determinations. 9,10-Diphenylanthracene as a reference standard in different solvents. *J. Phys. Chem.* **1976**, *80* (9), 969−974.
(38) Sk, B.; Ravindran, E.; Deori, U.; Yadav, N.; Nanda, G. P.; Rajamalli, P. A deep blue thermally activated delayed fluorescence emitter: balance between charge transfer and color purity. *J. Mater. Chem. C* **2022**, *10* (12), 4886−4893.
(39) Bandyopadhyay, S.; Kalangi, S. K.; Singh, V.; Bhosale, R. S. Chapter One—Introduction to aggregation induced emission (AIE) materials. In *Progress in Molecular Biology and Translational Science*; Bhosale, R. S., Singh, V., Eds.; Academic Press, 2021; Vol. *184*, pp 1−9.
(40) Greenspan, L. Humidity Fixed Points of Binary Saturated Aqueous Solutions. *J. Res. Natl. Bur. Stand. A Phys. Chem.* **1977**, *81A* (1), 89.
(41) Ma, X.; Sun, R.; Cheng, J.; Liu, J.; Gou, F.; Xiang, H.; Zhou, X. Fluorescence Aggregation-Caused Quenching versus Aggregation-Induced Emission: A Visual Teaching Technology for Undergraduate Chemistry Students. *J. Chem. Educ.* **2016**, *93* (2), 345−350.
(42) Mazumdar, A. K.; Nanda, G. P.; Yadav, N.; Deori, U.; Acharyya, U.; Sk, B.; Rajamalli, P. Thermally activated delayed fluorescence (TADF) emitters: sensing and boosting spin-flipping by aggregation. *Beilstein J. Org. Chem.* **2022**, *18*, 1177−1187.
(43) Pavia, D. L.; Lampman, G. M.; Kriz, G. S.; Vyvyan, J. A. *Introduction to Spectroscopy*; Cengage Learning, 2008.
(44) Huang, B.; Jiang, D.; Feng, Y.; Chen, W.-C.; Zhang, Y.; Cao, C.; Shen, D.; Ji, Y.; Wang, C.; Lee, C.-S. Mechanochromic luminescence and color-tunable light-emitting devices of triphenylamine functionalized benzo[d,e]benzo[4,5]imidazo[2,1-a]isoquinolin-7-one. *J. Mater. Chem. C* **2019**, *7* (32), 9808−9812.
(45) Im, Y.; Kim, M.; Cho, Y. J.; Seo, J.-A.; Yook, K. S.; Lee, J. Y. Molecular Design Strategy of Organic Thermally Activated Delayed Fluorescence Emitters. *Chem. Mater.* **2017**, *29* (5), 1946−1963.
(46) Wang, S.; Li, L.; Li, K.; Zhang, T.; Zhao, Z.; Xue, P. Mechanochromism of a dumbbell D−$\pi$−A−$\pi$−D phenothiazine derivative. *New J. Chem.* **2019**, *43* (33), 12957−12962.


https://doi.org/10.1021/acsmaterialsau.4c00036
*ACS Mater. Au* 2024, 4, 604−611